Influence of Flight Height on The Accuracy of UAV Derived Digital Elevation Model of Complex Terrain

Nguyen QUOC LONG[1,*], Ropesh GOYAL[2], Bui KHAC LUYEN[1], Le VAN CANH[1], Cao XUAN CUONG[1], Pham VAN CHUNG[1], Bui NGOC QUY[1], Xuan-Nam BUI[1]

[1] Hanoi University of Mining and Geology, 18 Vien street, Hanoi, 100000; email: nguyenquoclong@humg.edu.vn
[2] Indian Institute of Technology Kanpur, Kanpur-208016, Uttar Pradesh, India

http://doi.org/10.29227/IM-2020-01-27

Submission date: 16-03-2020 | Review date: 22-04-2020

Abstract

Lightweight Unmanned Aerial Vehicle (UAV) for 3D topographic mapping in mining industry has been raised significantly in recent years. Especially, in complex terrains such as in open-pit mines where the elevation is rapidly undulating, UAV-based mapping has proven its economic efficiency and higher safety compared to the conventional methods. However, one of the most important factors in UAV mapping of complex terrain is the flight altitude that needs to be considered seriously because of the safety of the instruments and the accuracy of generated DEMs. This paper aims to evaluate the influence of the flight height on the accuracy of DEMs generated in open-pit mines. To this end, the study area is selected in a quarry, with a complex terrain, located in northern Vietnam. The investigation was conducted with five flight heights of 50 m, 100 m, 150 m, 200 m, and 250 m. To assess the accuracy of resulting DEMs, ten high-precise and 385 precise checkpoints observed using GNSS/RTK and total station were used. The accuracy of DEM was assessed by root-mean-square error (RMSE) in X, Y, Z, XY, and XYZ components. The results show that DEM models generated at the flight heights of less than 150 m have high accuracy. RMSEs with the 10 high-precise checkpoints increase from 1.8 cm to 6.2 cm for the vertical (Z), and from 2.6 cm to 6.3 cm for the horizontal (XY), whereas RMSEs with 385 precise checkpoints increase gradually from 5 cm to 15 cm for the vertical (Z) when the flight height increases from 50 m to 250 m.

Keywords: *UAV, DEM, accuracy, complex terrain, quarry*

1. Introduction

Digital Elevation Model (DEM) or Digital Terrain Model (DTM) is a three-dimension (3D) representation of a bare-earth model (Guth, 2006), while Digital Surface Model (DSM) is a 3D representation of the Earth's surface, which includes all the canopies, buildings and other man-made features (Li, Zhu, & Gold, 2004). Both of the two models have their own specific applications (Fleming, Marsh, & Giles, 2010; Růžičková & Inspektor, 2015), but in open-pit mines, due to the absence of vegetation coverage or man-made features, DEM and DSM can be safely treated interchangeably as is done in this manuscript hereafter.

DEMs are important input for a wide range of applications in Earth sciences, e.g., gravity field or geological modeling, hydrological research, environmental studies, among others (Hirt, Filmer, & Featherstone, 2010). DEMs can be generated by various methods, including ground survey (e.g., (Heritage, Milan, Large, & Fuller, 2009)), terrestrial laser scanning (e.g., (Axelsson, 2000)), airborne photogrammetry (e.g., (Fabris & Pesci, 2005)), light detecting and ranging (LiDAR) (e.g., (Liu, 2008)), Unmanned Aerial Vehicles (UAVs) (e.g., (Uysal, Toprak, & Polat, 2015)), radar altimetry (e.g., (Hilton, Featherstone, Berry, Johnson, & Kirby, 2003)), and interferometric synthetic aperture radar (InSAR) (e.g., (Hanssen, 2001)).

In open-pit mines, a precise DEM is necessary for various applications, e.g., stockpile management, pit and dump management, slope stability, and mining-induced subsidence (Xiang, Chen, Sofia, Tian, & Tarolli, 2018). There are several global DEMs available in the public domain, such as Advanced Spaceborne Thermal Emission and Reflection Radiometer (ASTER) (Tachikawa et al., 2011) and Shuttle Radar Topography Mission (SRTM) (Farr et al., 2007). Although these DEMs have been used widely in various fields, e.g., hydrology, geophysics, environment, they are ineffectual in open-pit mines, where the landscape changes abruptly within a few meters, due to their coarse resolution (usually at 30 m or 90 m). Additionally, they are not updated frequently, and thus do not represent the most recent Earth's surface in mining areas, which is changing continuously during a mining project.

Local DEMs are therefore frequently employed in open-pit mines rather than a freely available global DEM. They are usually generated using either conventional surveying by, e.g., automatic levels or total stations, or more modern methods, which includes the use of 3D point cloud from LiDAR or UAVs photogrammetry. The conventional methods provide a high precision but have a

limitation of being labor-intensive with high cost and time. Hence, it is not a feasible method to generate an enormous number of DEMs required during the course of open-pit mining projects. Alternatively, LiDAR is an advanced technique for the rapid collection of the 3D point data of the topography, which is used to create reliable DEMs. However, the cost of collecting and processing the LiDAR data is very high, which may in turn increase the total cost of a project significantly. Conversely, UAV photogrammetry has been proven to be a suitable candidate technique for DEM generation in open-pit mines, which is neither comparatively labor intensive nor costly.

Recently, UAVs have been used extensively in many fields such as precise agriculture (Rokhmana, 2015), forestry (Paneque-Gálvez, McCall, Napoletano, Wich, & Koh, 2014), urban management (Salvo, Caruso, & Scordo, 2014), hazardous and environmental management (Chou, Yeh, Chen, & Chen, 2010; Gomez & Purdie, 2016; Lindner, Schraml, Mansberger, & Hübl, 2016; Lucieer, Jong, & Turner, 2014; Mourato, Fernandez, Pereira, & Moreira, 2017; Watson, Kargel, & Tiruwa, 2019), and mining industry (X. N. Bui et al., 2019). In mine surveying, many advantages of using lightweight UAVs have been proven, e.g., safety, accuracy, and productivity (Nguyen, Bui, Cao, & Le, 2019). It is also proven to be an efficient choice for generating intermittent DEMs due to regular excavations in open-pit mines (D. T. Bui et al., 2017). The safety and productivity of the UAV-based method are dependent on several factors, in which the flight altitude is one of the most important factors. This is due to the fact that the flight altitude has a direct impact on the resolution of UAV images in such a way that the higher the flight altitude is, the lower is the resolution of the generated DEM and vice-versa. This further affects the accuracy of the produced DEM.

From the safety perspective, the flight altitude needs to be considered seriously because the maximum flight altitude limitation is set by local authorities, whilst the minimum flight altitude depends on other factors, such as the accuracy requirement and the UAV take-off position. In terms of productivity, the amount of data captured and the processing time are inversely proportional to the flight height, and these factors may broadly correlate with the DEM accuracy as well. Therefore, a detailed investigation of the influence of the UAV flight height on the DEM accuracy is indispensable, especially when the UAV technique has been advocated as a better choice than others for efficient generation of multiple DEMs in a mining project.

There have been several studies on the influence of the UAV flight height on the accuracy of DEM (e.g., (Fuad et al., 2018; Mesas-Carrascosa, Notario García, Meroño de Larriva, & García-Ferrer, 2016; Udin & Ahmad, 2014; Yusoff, Darwin, Majid, Ariff, & Idris, 2018)), but, to the best of the authors' knowledge, none of the published studies include a terrain which is as complex as that investigated in this study. For example, Udin and Ahmad (2014) conducted experiments on a 200-m long stream with the water level being low and almost constant. They conducted experiments with varying flight altitudes of 40 m, 60 m, 80 m, and 100 m. Mesas-Carrascosa et al. (2016) evaluated the influence of the flight altitude on the accuracy of DEMs over the archaeological site in Torreparedones, southern Spain, with flight altitudes varying between 30 m and 80 m above ground level.

In this study, we provide a detailed analysis of the influence of the flight height on the DEM accuracy with rigorous experiments conducted in an open-pit mine in Vietnam, which has rapidly undulating terrains. Five different DEMs are constructed using UAV data with the flight heights being 50 m, 100 m, 150 m, 200 m, and 250 m. The remainder of this study is organized as follow: In the next section, the study area and methodology are discussed, which are followed by the results and discussions in Section 3. The conclusions of the study are provided in Section 4.

2. Study area and data collection

Study area:

This study is conducted in the mining site of Long Son limestone quarry that belongs to the Long Son cement plant. This quarry is located in Ha Vinh commune, Ha Trung district, Thanh Hoa province, which is about 200 km away from Hanoi, Vietnam. It encloses an area of about 1 km^2 with topographical characteristics of a quarry similar to many other quarries in northern Vietnam, including benches, the toe of the benches, and steep slopes. At the time of the study, the mine had already gone through the stage of basic construction and was at an excavating level of 110 m (Fig. 1).

Survey flight:

To collect aerial data, a commercial quadcopter DJI Phantom 4 Pro mounting a 20-megapixel RGB camera with a focal length of 8.8 mm and a sensor size of 13.2 mm x 8.8 mm (https://www.dxomark.com) that allows high-resolution aerial photography is employed. Its airframe carries a GPS/IMU that enables it to have a posture control, stop flight, and automatically take off and land with high stability. The drone operates in both manual flight mode using a controller and automatic flight mode using an Android or IOS smartphone. In this study, we use Pix4Dcapture software installed on an iPhone 7 plus for planning the flight. In the automatic mode, several vital parameters are set to the drone, including a mapping area of 1 km^2, a flight height, forward overlap, and side-lap of 80%. The position of each camera was measured at the time of data capturing by a low-cost GNSS/INS receiver mounted on the drone, with an average accuracy of 2.5 m along the axes. This information is stored in each image's file and used for processing imagery to obtain photogrammetric products.

To assess the influence of flight heights on the accuracy of the DEM, we flew the Phantom 4 Pro at five different altitudes above ground level: 50 m, 100 m, 150 m, 200 m and 250 m with average Ground Sample Distance (GSD) of 1.36, 2.73, 4.09, 5.45, 6.82 cm/pix, respectively. The take-off location of the UAV is chosen to ensure safety, especially when flying at low altitudes. In this study, we choose the take-off location located at the middle high of the study area, with an elevation of 80 m above sea level. This ensured that when we fly the UAV at the lowest altitude of 50 m, the UAV is safe from the highest point in the study area (Fig. 2b).

Fig. 1. The location of Long Son quarry
Rys. 1. Lokalizacja kamieniołomu Long Son

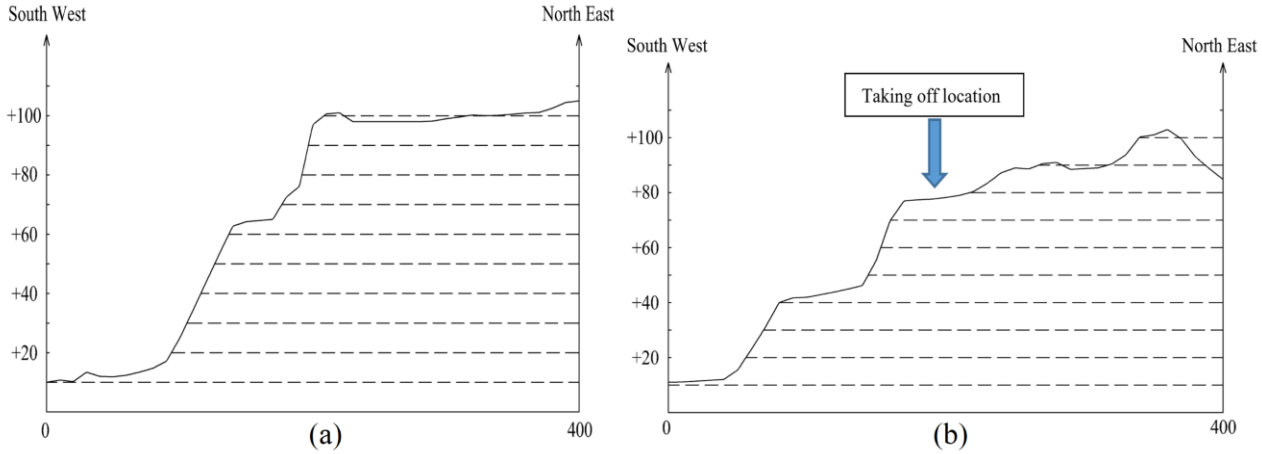

Fig. 2. The profiles of study area: Profile I-I (a), Profile II-II (b)
Rys. 2. Profile obszaru badań: Profil I-I (a), Profil II-II (b)

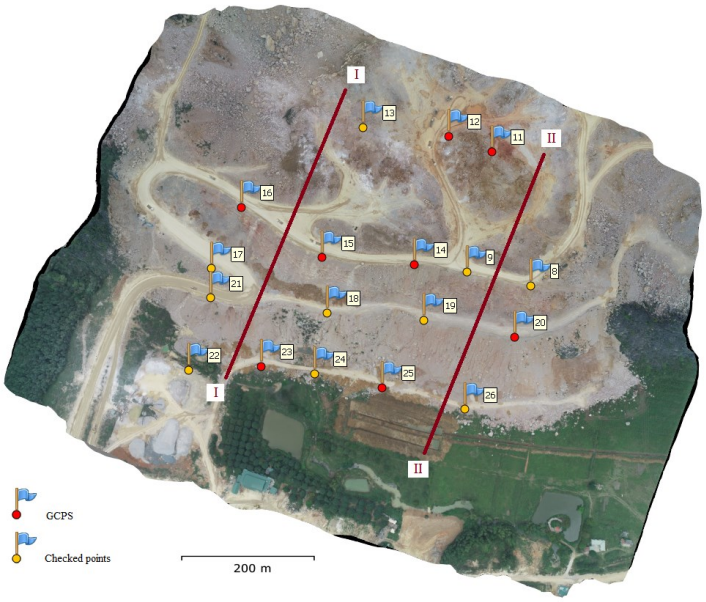

Fig. 3. Distribution of GCPs and high-precise check points along with the location of profiles
Rys. 3. Rozkład punktów kontrolnych i kontrolowanych oraz lokalizacja profili

Establishing the Ground Control Points:

Ground Control Points (GCPs) play an essential role in geo-referencing and evaluating the accuracy of DEMs. Therefore, the acquisition of GCPs needs to be planned before carrying out image acquisition. In a condition when the quarry was still operating, field reconnaissance with handheld GPS is conducted to select safe areas for establishing the GCPs. A total of 18 GCPs were placed at various heights and uniformly distributed to cover the entire area. Of these 18 GCPs, eight were used for the calibration (camera-lens optimization and bundle block adjustment) and generation of the different DEMs, while ten GCPs were used as high-precise check points (Fig. 3). These were measured by dual-frequency GNSS/RTK receivers (Fig. 4). The specifications of GNSS receivers are listed in Table 1. In addition, to better assess the accuracy of DEMs, 305 precise check points were observed using the GNSS-RTK mode in the study area on the main features, including benches and the toe of the benches. Furthermore, 80 precise check points were measured using total station in non-prism mode over the area on slopes as these areas are more complex and cannot be accessed in person. The expected accuracy in elevation of these measurements is about 1-1.5 cm. A Leica TS02 total station with an angular accuracy of 5" and a distance accuracy of 1.5 mm + 2 ppm was used (Fig. 4).

The GCPs and check points are marked on the ground with the size of 60x60 cm targets which were designed in black and yellow with a highly reflective material. The coordinates of GCPs were measured in the national control network (the VN2000 coordinate system), using the GNSS/RTK method. The base receiver was installed at one control point of the national control network established in the local area; the rover measured each point with a pole clip to ensure stability. Each point was measured at least three times, and after eliminating rough errors, the final point coordinates were the average value. Any GCPs that did not satisfy the accuracy were removed, and the remaining points were used to calibrate the camera and evaluate the accuracy of models.

Tab. 1. The specifications of CHC X91 GNSS Receiver and Leica TS02
Tab. 1. Specyfikacje odbiornika CHC X91 GNSS i Leica TS02

CHC X91 GNSS Receiver	Leica TS02
- Horizontal: + (10mm + 1ppm) RMS - Vertical: +(20mm + 1ppm) RMS - Initializing Time: Typical >99.9% - Static: Horizontal: + (5mm + 1ppm) RMS Vertical: +(10mm + 1ppm) RMS	- 5″ Angle measurement accuracy - 3500m Single prism range - R500 EDM – 500m reflector less range - Pinpoint EDM – The most precise in its class (1.5mm + 2ppm)

Fig 4. Observing GCPs and check points using the GNSS and total station.
Rys. 4. Ustanowienie punktów kontroli naziemnej za pomocą metod GNSS i tachimetru

Software and image processing:

In this study, Agisoft Photoscan Professional (ver 1.54) was used to process UAV images acquired in the field. The data processing procedure of Agisoft Photoscan includes five steps: (i) photo alignment; (ii) bundle block adjustment; (iii) optimization, (iv) 3D surface reconstruction, (v) generation of DSM. Firstly, when images are inputted, the key points that can be easily identified from each image are automatically extracted. The singularities extracted from each image are then linked with each other through mutual comparison among a plurality of images. This process is called "photo alignment". When geometric corrections of singularities are completed in each image, the singularities representing the same points in several images are automatically matched through a comparison between consecutive UAV

images. Once the singularities are extracted, the 3D point cloud and the DSM are generated.

Evaluation Methods:

The goal of this study is to evaluate the accuracy of DEM generated using UAV dataset with different flight altitudes. For this, the block orientation quality was first assessed on 10 signalized 3D check points. Further, the DEMs were evaluated by comparing the observed and extracted elevation values at a broader set of check points using the different values and the Root Mean Square Error (RMSE) given by Eqs.1-6.

$$\Delta X = \mathrm{X_{DEM}} - \mathrm{X_{GCP}};\ \Delta Y = \mathrm{Y_{DEM}} - \mathrm{Y_{GCP}};$$
$$\Delta Z = \mathrm{Z_{DEM}} - \mathrm{Z_{GCP}};\ \Delta XY = \mathrm{XY_{DEM}} - \mathrm{XY_{GCP}} \quad (1)$$
$$\Delta XYZ = \mathrm{XYZ_{DEM}} - \mathrm{XYZ_{GCP}}$$

$$RMSE_X = SQRT\left[(1/n)\sum_{i=1}^{n}(X_{DEM} - X_{GCPi})^2\right] \quad (2)$$

$$RMSE_Y = SQRT\left[(1/n)\sum_{i=1}^{n}(Y_{DEM} - Y_{GCPi})^2\right] \quad (3)$$

$$RMSE_{XY} = SQRT\left[(1/n)\sum_{i=1}^{n}(\Delta X)^2 + (\Delta Y)^2\right] \quad (4)$$

$$RMSE_Z = SQRT\left[(1/n)\sum_{i=1}^{n}(\Delta Z)^2\right] \quad (5)$$

$$RMSE_{XYZ} = SQRT\left[(1/n)\sum_{i=1}^{n}((\Delta X)^2 + (\Delta Y)^2 + (\Delta Z)^2)\right] \quad (6)$$

where $\mathrm{X_{GCPi}}$ and $\mathrm{X_{DSM}}$ are the X-coordinate of GCP and corresponding coordinate in DEM, respectively; $\mathrm{Y_{GCPi}}$ and $\mathrm{Y_{DSM}}$ are the Y-coordinate of GCP and corresponding coordinate in DEM, respectively; $\mathrm{Z_{GCPi}}$ and $\mathrm{Z_{DSM}}$ are the Z-coordinate of GCP and corresponding coordinate in DEM, respectively.

3. Results and Discussions

The accuracy assessments of the camera-lens model calibration and the DEM with eight GCPs and 10 high-precise check points for 50 m flight height are summarized in Tables 2 and 3, respectively. The RMSEs in different directional components for the GCPs and high precise check points, with respect to the five different flight heights, are summarized in Table 4 and graphically represented in Figure 5.

At the flight height of 50 m, the largest number of images (247) with a resolution of 1.36 cm/pixel were acquired. The point cloud of the quarry with approximately 101,982 3D points was extracted following the method described above. Further, an orthographic image and a DEM were generated with resolutions of 1.3 cm and 13.3 cm, respectively. Table 2 shows that the accuracy of the model built from the calibrating dataset is much reliable with all the errors within 1 cm. However, it may be too optimistic as the calibrating dataset was used for both the optimization process and the accuracy assessment. Therefore, the check-point dataset was used to assess the accuracy of the DEM model. In Table 3, it could be seen that the maximum error for X is -3.9 cm (GCP9), Y is 3.4 cm (GCP19), Z is 3.1 cm (GCP17), XY is 3.9 cm (GCP9), and XYZ is 4.7 cm (GCP17). With a DEM of 13.3 cm resolution, the $\mathrm{RMSE_{XY}}$ of 2.6 cm and $\mathrm{RMSE_Z}$ of 1.8 cm indicates the appropriate reliability of the constructed DEM to be used in open-pit mining applications.

From Table 4 and Figure 5a, it is observed that the RMSEs in X, Y, XY, Z, XYZ are smallest with 0.2 cm, 0.3 cm, 0.4 cm, 0.5 cm, and 0.6 cm, respectively for the 50 m flight altitude, whereas with 250 m flight altitude RMSEs in X, Y, XY, Z, XYZ are largest having the values 5.2 cm, 6.0 cm, 7.9 cm, 8.5 cm, and 10.6 cm. Figure 5b shows that for the check-point dataset also the smallest and largest RMSEs in X, Y, XY, Z and XYZ are with the flight altitudes of 50 m and 250 m, respectively. Thus, we obtain an indirect proportionality between the flight altitude and the DEM accuracy. This is further confirmed by validating the five DEMs with respect to 385 precise check points measured on benches, the toe of the benches and steep slopes. Figure 6 depicts that, with 385 precise check points, the DEM vertical error increases gradually from 0.05 m to 0.15 m when the flight height increases from 50 m to 250 m. The results of the present study show a similarity with the results reported by Udin and Ahmad (2014), Mesas-Carrascosa et al. (2016), Fuad et al. (2018) and Yusoff et al. (2018), but a different result compared some studies which reported that the horizontal accuracy is not affected by flight altitude and terrain morphology.

Tab. 2. Difference and RMSE of 8 GCPs used for the model calibration (the flight height of 50 m)
Tab. 2. Błąd i RMSE GCP stosowanych do kalibracji modelu (wysokość lotu 50 m)

Label	ΔX (cm)	ΔY (cm)	ΔXY (cm)	ΔZ (cm)	ΔXYZ (cm)
11	0.2	-0.1	0.2	-0.3	0.4
12	-0.3	0.1	0.3	0.2	0.4
14	0.2	-0.4	0.4	0.9	1.0
15	-0.3	-0.1	0.3	-0.8	0.8
16	0.1	0.2	0.2	0.0	0.2
20	0.1	0.5	0.5	-0.1	0.5
23	0.2	0.2	0.3	0.3	0.4
25	-0.3	-0.4	0.5	-0.3	0.6
RMSE	0.2	0.3	0.4	0.5	0.6

Tab 3. Difference and RMSE of 10 high-precise check points (the flight height of 50 m)
Tab. 3. Błąd i RMSE punktów kontrolnych (wysokość lotu 50 m)

Label	ΔX (cm)	ΔY (cm)	ΔXY (cm)	ΔZ (cm)	ΔXYZ (cm)
13	-1.4	-0.3	1.4	1.2	1.9
17	3.5	-0.4	3.5	3.1	4.7
18	0.8	2.0	2.2	1.1	2.5
19	0.1	3.4	3.4	0.9	3.6
21	3.0	0.9	3.1	0.0	3.2
22	-0.8	1.0	1.3	-2.8	3.1
24	-1.0	1.2	1.6	-2.6	3.0
26	0.8	-1.1	1.4	-1.7	2.1
8	-2.1	-1.9	2.8	0.1	2.9
9	-3.9	-0.2	3.9	-1.2	4.0
RMSE	2.1	1.6	2.6	1.8	3.2

Tab 4. The summary of accuracy assessment of DEMs generated at five flight heights
Tab. 4. Podsumowanie dokładności DEM wygenerowanej dla pięciu wysokości lotu

Flight Height (m)	RMSE Ground Control Points (cm)					RMSE Check points (cm)				
	ΔX	ΔY	ΔXY	ΔZ	ΔXYZ	ΔX	ΔY	ΔXY	ΔZ	ΔXYZ
50	0.2	0.3	0.4	0.5	0.6	2.1	1.6	2.6	1.8	3.2
100	0.9	1.2	1.5	2.0	2.0	3.5	2.2	4.1	3.8	4.0
150	2.0	2.8	3.4	4.4	5.2	5.0	3.9	6.3	6.2	7.1
200	3.5	4.0	5.3	5.8	6.7	6.5	6.0	8.8	8.1	10.9
250	5.2	6.0	7.9	8.5	10.6	8.2	9.0	12.2	12.5	16.6

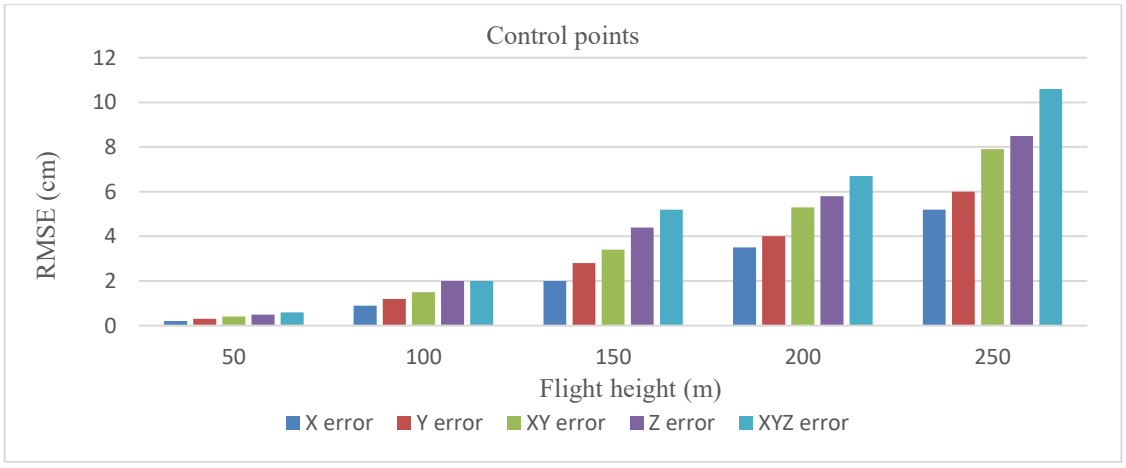

(a)

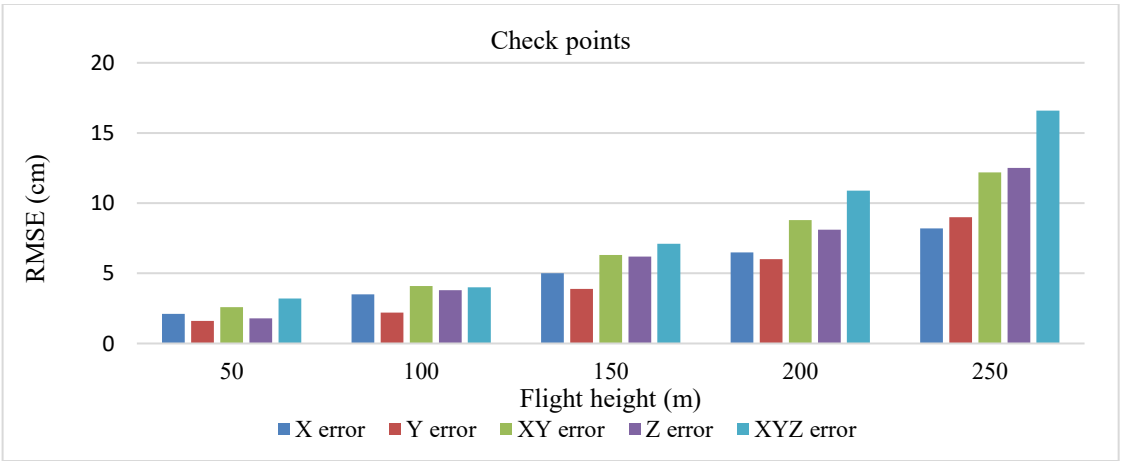

(b)

Fig. 5. Root Mean Square Errors (RMSEs) of GCPs for camera calibration (a) and checkpoints for DEM accuracy (b)
Rys. 5. Średnie kwadratowe błędy pierwiastkowe (RMSE) na GCP do kalibracji kamery (a) i punktów kontrolnych dla dokładności DEM (b)

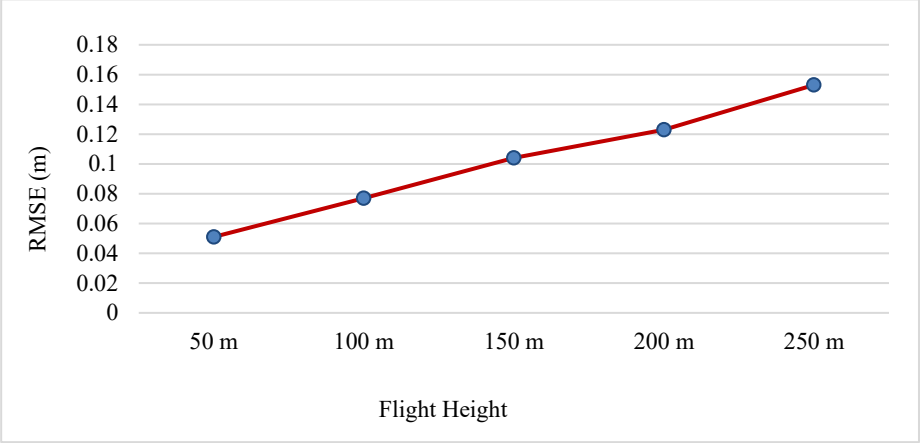

Fig. 6. DEM vertical error with respect to the 385 precise checkpoints (for each flight height)
Rys. 6. Średnie wartości błędu DEM przy użyciu GNSS/RTK i punktów kontrolnych tachimetru dla każdej wysokości lotu

4. Conclusions

An experimental investigation on the accuracy of DEMs generated using UAV datasets was performed. The data was collected with UAV at five different altitudes, i.e., 50 m, 100 m, 150 m, 200 m and 250 m above ground level over complex terrains of quarry. Accordingly, a lightweight and the 1-inch EXMOR R CMOS camera mounted on a low-cost DJI Phantom 4 Professional UAV was used. The acquired number of images increased from 80 to 247, with a decrease in the flight altitude from 250 m to 50 m. The processing was carried out using 8 GCPs. While the accuracy assessment was done using 10 high-precise and 385 precise check points.

The results showed that the accuracy of DEM is reliable, with flight height ranging between 50 m to 250 m. However, it is important to note here again that we have used a total of 8 GCPs for processing the UAV dataset. With the variation of flight altitude from 50 m to 250 m, RMSE in the calibrating dataset increases from 0.5 cm to 8.5 cm for vertical, and from 0.4 cm to 7.9 cm for horizontal, indicating high success-rate of fit in processing, whereas RMSE in the check-point dataset increases from 1.8 cm to12.5 cm for vertical, and from 2.6 cm to 12.2 cm for horizontal, indicating high accuracy. These indicate that the processes of capturing images, the establishment of GCPs, and photogrammetric processing were carried out successfully. Also, it is concluded that the altitude of the drone influences both horizontal and vertical accuracy of DEM. The greater the flight height is, the lower the accuracy of the DEM model.

Acknowledgments

This research was supported financially by the Ministry of Education and Training of Vietnam (MOET) project B2020-MDA-14.

Literatura – References

1. Axelsson, P. (2000). DEM generation from laser scanner data using adaptive TIN models. International archives of photogrammetry and remote sensing, 33(4), 110-117.
2. Bui, D. T., Long, N. Q., Bui, X.-N., Nguyen, V.-N., Van Pham, C., Van Le, C., . . . Kristoffersen, B. (2017). Lightweight unmanned aerial vehicle and structure-from-motion photogrammetry for generating digital surface model for open-pit coal mine area and its accuracy assessment. Paper presented at the International Conference on Geo-Spatial Technologies and Earth Resources.
3. Bui, X. N., Lee, C., Nguyen, Q. L., Adeel, A., Cao, X. C., Nguyen, V. N., . . . Duong, T. H. (2019). Use of Unmanned Aerial Vehicles for 3D topographic Mapping and Monitoring the Air Quality of Open-pit Mines. Inżynieria Mineralna, 21.
4. Chou, T.-Y., Yeh, M.-L., Chen, Y. C., & Chen, Y. H. (2010). Disaster monitoring and management by the unmanned aerial vehicle technology. In: Wagner W., Székely, B. (eds.), ISPRS TC VII Symposium – 100 Years ISPRS, Vienna, Austria, July 5–7, 2010, IAPRS, Vol. XXXVIII, Part 7B
5. Fabris, M., & Pesci, A. (2005). Automated DEM extraction in digital aerial photogrammetry: precisions and validation for mass movement monitoring. Annals of Geophysics, 48(6), 973-988. doi: 10.4401/ag-3247
6. Farr, T. G., Rosen, P. A., Caro, E., Crippen, R., Duren, R., Hensley, S., . . . Roth, L. (2007). The shuttle radar topography mission. Reviews of geophysics, 45(2), RG2004. doi: 10.1029/2005RG000183
7. Fleming, C., Marsh, S., & Giles, J. (2010). Introducing elevation models for geoscience. Geological Society, London, Special Publications, 345(1), 1-4. doi: 10.1144/SP345.1
8. Fuad, N., Ismail, Z., Majid, Z., Darwin, N., Ariff, M., Idris, K., & Yusoff, A. (2018). Accuracy evaluation of digital terrain model based on different flying altitudes and conditional of terrain using UAV LiDAR technology. Paper presented at the IOP conference series: earth and environmental science. doi: 10.1088/1755-1315/169/1/012100
9. Gomez, C., & Purdie, H. (2016). UAV-based photogrammetry and geocomputing for hazards and disaster risk monitoring–a review. Geoenvironmental Disasters, 3, 23. doi: 10.1186/s40677-016-0060-y
10. Guth, P. L. (2006). Geomorphometry from SRTM. Photogrammetric Engineering & Remote Sensing, 72(3), 269-277. doi:10.14358/pers.72.3.269
11. Hanssen, R. (2001). Radar Interferometry: Data Interpretation and Error Analysis Remote Sensing and Digital Image Processing (Vol. 2, pp. XVIII, 308): Springer Netherlands.
12. Heritage, G. L., Milan, D. J., Large, A. R., & Fuller, I. C. (2009). Influence of survey strategy and interpolation model on DEM quality. Geomorphology, 112(3-4), 334-344. doi:10.1016/j.geomorph.2009.06.024
13. Hilton, R., Featherstone, W., Berry, P., Johnson, C., & Kirby, J. (2003). Comparison of digital elevation models over Australia and external validation using ERS-1 satellite radar altimetry. Australian Journal of Earth Sciences, 50(2), 157-168. doi:10.1046/j.1440-0952.2003.00982.x
14. Hirt, C., Filmer, M. S., & Featherstone, W. E. (2010). Comparison and validation of the recent freely available ASTER-GDEM ver1, SRTM ver4.1 and GEODATA DEM-9s ver3 digital elevation models over Australia. Australian Journal of Earth Sciences, 57(3), 337-347. doi:10.1080/08120091003677553
15. https://www.dxomark.com.
16. Li, Z., Zhu, C., & Gold, C. (2004). Digital terrain modeling: principles and methodology: CRC press.
17. Lindner, G., Schraml, K., Mansberger, R., & Hübl, J. (2016). UAV monitoring and documentation of a large landslide. Applied Geomatics, 8(1), 1-11. doi: 10.1007/s12518-015-0165-0
18. Liu, X. (2008). Airborne LiDAR for DEM generation: Some critical issues. Progress in Physical Geography, 32(1), 31-49. doi:10.1177/0309133308089496
19. Lucieer, A., Jong, S. M. d., & Turner, D. (2014). Mapping landslide displacements using Structure from Motion (SfM) and image correlation of multi-temporal UAV photography. Progress in Physical Geography, 38(1), 97-116. doi: 10.1177/0309133313515293
20. Mesas-Carrascosa, F.-J., Notario García, M. D., Meroño de Larriva, J. E., & García-Ferrer, A. (2016). An analysis of the influence of flight parameters in the generation of unmanned aerial vehicle (UAV) orthomosaicks to survey archaeological areas. Sensors, 16(11), 1838. doi: 10.3390/s16111838
21. Mourato, S., Fernandez, P., Pereira, L., & Moreira, M. (2017). Improving a DSM obtained by unmanned aerial vehicles for flood modelling. Paper presented at the IOP Conference Series: Earth and Environmental Science. doi: 10.1088/1755-1315/95/2/022014
22. Nguyen, Q. L., Bui, X. N., Cao, X. C., & Le, V. C. (2019). An approach of mapping quarries in Vietnam using low-cost Unmanned Aerial Vehicles. Sustainable Development of Mountain Territores, T.11. N-2(40), 199-209. doi: 10.21177/1998-4502-2019- 11-2-199-210
23. Paneque-Gálvez, J., McCall, M. K., Napoletano, B. M., Wich, S. A., & Koh, L. P. (2014). Small drones for community-based forest monitoring: An assessment of their feasibility and potential in tropical areas. Forests, 5(6), 1481-1507. doi: 10.3390/f5061481

24. Rokhmana, C. (2015). The potential of UAV-based remote sensing for supporting precision agriculture in Indonesia. Procedia Environmental Science, 24, 245–253. doi: 10.1016/j.proenv.2015.03.032
25. Růžičková, K., & Inspektor, T. (2015). Surface Models for Geosciences: Springer, Switzerland.
26. Salvo, G., Caruso, L., & Scordo, A. (2014). Urban traffic analysis through an UAV. Procedia-Social and Behavioral Sciences, 111, 1083-1091. doi: 10.1016/j.sbspro.2014.01.143
27. Tachikawa, T., Kaku, M., Iwasaki, A., Gesch, D., Oimoen, M., Zhang, Z., . . . Haase, J. (2011). ASTER Global Digital Elevation Model Version 2–Summary of Validation Results.
28. Udin, W., & Ahmad, A. (2014). Assessment of photogrammetric mapping accuracy based on variation flying altitude using unmanned aerial vehicle. Paper presented at the IOP conference series: earth and environmental science.doi: 10.1088/1755-1315/18/1/012027
29. Uysal, M., Toprak, A. S., & Polat, N. (2015). DEM generation with UAV Photogrammetry and accuracy analysis in Sahitler hill. Measurement, 73, 539-543. doi:10.1016/j.measurement.2015.06.010
30. Watson, C. S., Kargel, J. S., & Tiruwa, B. (2019). UAV-derived himalayan topography: hazard assessments and comparison with global DEM products. Drones, 3(1), 18. doi: 10.3390/drones3010018
31. Xiang, J., Chen, J., Sofia, G., Tian, Y., & Tarolli, P. (2018). Open-pit mine geomorphic changes analysis using multi-temporal UAV survey. Environmental Earth Sciences, 77(6), 220. doi:10.1007/s12665-018-7383-9
32. Yusoff, A., Darwin, N., Majid, Z., Ariff, M., & Idris, K. (2018). Comprehensive analysis of flying altitude for high resolution slope mapping using UAV technology. International Archives of the Photogrammetry, Remote Sensing and Spatial Information Sciences, 42(3/W4), 583-589. doi: 10.5194/isprs-archives-XLII-3-W4-583-2018

Wysokość lotu UAV i jego wpływ na precyzyjny cyfrowy model wysokości złożonego terenu

Zastosowanie lekkich bezzałogowych statków powietrznych (UAV) jest coraz bardziej powszechne w badaniach topograficznych 3D. Zwłaszcza w skomplikowanych terenach, takich jak kopalnie odkrywkowe, w których wzniesienie gwałtownie faluje, mapowanie oparte na UAV jest bardziej wydajne, ekonomiczne i bezpieczne w porównaniu z metodami konwencjonalnymi. Jednak jednym z najważniejszych czynników w mapowaniu UAV złożonego terenu jest wysokość lotu, którą należy poważnie rozważyć ze względu na bezpieczeństwo i dokładność generowanych DEM. Niniejszy artykuł ma na celu ocenę wpływu wysokości lotu na dokładność DEM generowanych dla kopalni odkrywkowych. W tym celu wybranym obszarem badawczym jest kamieniołom o złożonym terenie położony w północnym Wietnamie. Badanie przeprowadzono przy pięciu wysokościach lotu 50 m, 100 m, 150 m, 200 m i 250 m. Aby ocenić dokładność uzyskanych DEM, wykorzystano 10 naziemnych punktów kontrolnych i 385 punktów kontrolnych mierzonych zarówno metodami GNSS/RTK, jak i metodami stacji całkowitej. Dokładność DEM oceniono za pomocą błędu pierwiastkowego średniego kwadratu (RMSE) w komponentach X, Y, Z, XY i XYZ. Wynik pokazał, że modele DEM generowane na wysokościach lotu poniżej 150 m mają wysoką dokładność, RMSE na 10 GCP wzrosły z 1,8 cm do 6,2 cm dla pionu (Z) i od 2,6 cm do 6,3 cm dla poziomu (XY), podczas gdy RMSE na 385 punktach kontrolnych wzrasta stopniowo z 0,05 m do 0,15 m dla pionu (Z), gdy lot na wysokości wzrósł z 50 m do 250 m.

Słowa kluczowe: *UAV, DEM, dokładność, złożony teren, kopalnie odkrywkowe*